Distinct RopGEFs successively drive polarization and outgrowth of root hairs

AUTHORS:

Philipp Denninger[1,6], Anna Reichelt[1,6], Vanessa A. F. Schmidt[1], Dietmar G. Mehlhorn[3], Lisa Y. Asseck[3], Claire E. Stanley[4,5], Nana F. Keinath[1], Jan-Felix Evers[1], Christopher Grefen[3] and Guido Grossmann[1,2,*]

AFFILIATIONS:

[1]Centre for Organismal Studies (COS), Heidelberg University, Im Neuenheimer Feld 230, 69120 Heidelberg, Germany

[2]Excellence Cluster CellNetworks, Heidelberg University, Im Neuenheimer Feld 267, 69120 Heidelberg, Germany

[3]Center for Plant Molecular Biology, Developmental Genetics, University of Tübingen, Auf der Morgenstelle 32, 72076 Tübingen, Germany

[4]Institute for Chemical and Bioengineering, ETH Zürich, Vladimir-Prelog-Weg 1, 8093 Zürich, Switzerland

[5]Agroecology and Environment Research Division, Agroscope, Reckenholzstrasse 191, 8046 Zürich, Switzerland

[6]These authors contributed equally.

*Correspondence:
Guido Grossmann
Centre for Organismal Studies
Im Neuenheimer Feld 230
69120 Heidelberg
Germany
email: guido.grossmann@cos.uni-heidelberg.de
ORCID ID: 0000-0001-7529-9244

SUMMARY

Root hairs are tubular protrusions of the root epidermis that significantly enlarge the exploitable soil volume in the rhizosphere. Trichoblasts, the cell type responsible for root hair formation, switch from cell elongation to tip growth through polarization of the growth machinery to a pre-defined root hair initiation domain (RHID) at the plasma membrane. The emergence of this polar domain resembles the establishment of cell polarity in other eukaryotic systems [1-3]. Rho-type GTPases of plants (ROPs) are among the first molecular determinants of the RHID [4, 5] and later play a central role in polar growth [6]. Numerous studies have elucidated mechanisms that position the RHID in the cell [7-9] or regulate ROP activity [10-18]. The molecular players that target ROPs to the RHID and initiate outgrowth, however, have not been identified. We dissected the timing of the growth machinery assembly in polarizing hair cells and found that positioning of molecular players and outgrowth are temporally separate processes that are each controlled by specific ROP guanine nucleotide exchange factor (GEFs). A functional analysis of trichoblast-specific GEFs revealed GEF3 to be required for normal ROP polarization and thus efficient root hair emergence, while GEF4 predominantly regulates subsequent tip growth. Ectopic expression of GEF3 induced the formation of spatially confined, ROP-recruiting domains in other cell types, demonstrating the role of GEF3 to serve as a membrane landmark during cell polarization.

RESULTS AND DISCUSSION

Temporal analysis of hair cell polarization reveals phased deployment of the tip-growth machinery

To dissect the process of breaking cellular symmetry and initiating polar growth in plants, we analyzed the gradual assembly of the tip growth machinery in trichoblasts using specific markers for cytoskeletal rearrangement, plasma membrane specialization, cell wall modification, vesicle trafficking, and Rho-GTPase signaling. Using stable transgenic *Arabidopsis* lines expressing fluorescently labeled versions of these protein markers, we determined the timing of their polarization at the RHID during trichoblast differentiation. As the *Arabidopsis* root represents a time-axis of development from stem cells to mature cells, we numbered the developmental stages (-7 to +3) within a cell file, with the last cell before bulging labeled -1 and the first cell after the onset of bulging labeled +1 (**Figure 1A**). We used the integral plasma membrane marker GFP-LTI6B [19] as a reference and calculated the polarity index of fluorescently labeled marker proteins to quantify protein accumulation at the RHID (**Figure 1B, C**). Our survey unveiled a two-phase assembly of the tip growth machinery: an initiation phase, during which the RHID is positioned and predefined, followed by the tip growth phase. Consistent with previous reports [4, 5], mCitrine-labeled (mCit) GTPase ROP2 associated with the RHID during the early initiation phase (stage -4), well before any detectable cell bulging (**Figure 1B-D, Figure S1**). The timing of mCit-ROP2 polarization appeared to be largely independent from promoter activity, as analysis of an estradiol-inducible reporter construct for mCit-ROP2 resulted in a similar timing of RHID association, albeit with higher cytosolic signal (**Figure 1D, Figure S1**). Closely related GTPases ROP4 and ROP6 exhibited a similar timing as ROP2, when inducibly expressed (**Figure 1D, Figure S1**), which indicates that ROP GTPases are prepositioned well before growth is activated. The only tested ROP-effectors that were found to polarize after ROPs but still during the initiation phase, were the PHOSPHATIDYLINOSITOL-4-PHOSPHATE 5-KINASE 3 (PIP5K3) [20], and the NADPH oxidase ROOT HAIR DEFECTIVE 2 (RHD2) [21, 22]. PIP5K3 and RHD2 have both been shown to directly interact with ROPs during tip growth regulation [18, 23] and modulate vesicle traffic to the plasma membrane and cell wall rigidity, respectively [24].

The second phase of root hair emergence was characterized by the polarization of known ROP effectors such as (ARPC2), a subunit of the actin polymerizing ARP2/3 complex [25], and the markers for vesicle transport and secretion SYP123 and SEC3A [26-28] (**Figure 1D, Figure S1**). The onset of bulge formation was further characterized by local elevation of cytosolic Ca^{2+} as reported by the sensor RGECO-1 [29, 30], as well as the formation of $PI(4,5)P_2$ at the emerging apex as indicated by the reporter P15Y [31]. The receptor-like kinase FERONIA, which activates ROPs during root hair tip growth [32], accumulated after bulging in stage +2 (**Figure 1D, Figure S1**). Even though our visualization of total ROP distribution does not provide information on the ROP activity state, the temporal separation of ROP positioning and growth activation led us to

hypothesize that distinct upstream, phase-specific regulators drive ROP GTPase recruitment and activation.

RopGEFs exhibit specific spatiotemporal patterns of expression and subcellular localization

ROPs have been extensively studied during cell elongation [33], stomata regulation [34], pavement cell development [35, 36], and in regulation of the two tip-growing plant cell types, pollen tubes [37] and root hairs [4, 5]. As molecular “switches”, the activity-state of GTPases depends on regulators that “toggle” the switch between active or inactive [38, 39]. GTPase-activating proteins (GAPs) accelerate hydrolysis of a bound GTP to GDP, rendering the GTPase inactive. Examples for GAPs with described roles in pollen tube growth are RopGAP1 [40] and REN1 [14]. To switch the GTPase into an active state, guanyl-nucleotide exchange factors (GEFs) facilitate GDP release from the GTPase and the binding of another GTP molecule, and thereby promote interactions with downstream effectors [39, 41]. RopGEFs of the PRONE family [42, 43] and SPK1, the only DOCK family GEF [44], play known roles in tip growth regulation in pollen tubes [17, 45, 46] and leaf trichomes[44, 47]. However, temporal relationships between ROPs and RopGEFs have not yet been established in these cell types and much less is known about RopGEF functions in root hairs.

To identify candidate ROP regulators that play potential roles in root hair initiation and growth regulation we mined cell-type-specific gene expression data [48-50] and compared expression profiles of RopGEFs in root trichoblasts and atrichoblasts. Among these RopGEFs (hereafter abbreviated as GEFs), the expression of GEF3 and GEF4 showed the strongest root hair-specificity, followed by GEF12, GEF11, GEF14, and GEF10 in descending order (**Figure S2A**). Based on their trichoblast-specific expression, these GEFs were selected for subsequent analyses. To determine in which stage of hair cell maturation the candidate GEFs play their roles, we analyzed their expression patterns in growing roots expressing mCit fusions under the control of the respective native promoters. We observed a diverse distribution of expression patterns among the remaining GEFs, with a surprisingly unique pattern for each gene (**Figure 2A**). We further analyzed the timing of polarization at the RHID for each mCit-labeled GEF and compared it to the timing of mCit-ROP2. We found that mCit-GEF3 and mCit-GEF14 reached significant polarization consistently one cell stage earlier than mCit-ROP2 (**Figure 2B, Figure S1**). A major difference between both expression patterns was that GEF14 expression lasted from the meristematic zone (MZ) to the elongation zone (EZ), whereas GEF3 expression was first observed in the root transition zone (TZ, in-between MZ and EZ) and lasted beyond hair emergence (**Figure 2A**). The beginning of gene expression of GEF4 and GEF12 was detected first in EZ and the polarization of both proteins at the RHID coincided with the onset of bulge formation (**Figure 2A, B, Figure S1**). This specific expression pattern and the timing of polarization of both, GEF4 and GEF12, indicate similar functions during a defined time window in differentiating trichoblasts. This is distinctly different compared to GEF3 and GEF14, as these GEFs both polarize at a significantly earlier timepoint and show a more defined and restricted localization to the RHID.

129 In addition to the specific expression pattern of GEF3, its localization stood out in comparison
130 to all other GEFs, as mCit-GEF3 appeared highly polarized at the cell periphery of the RHID, soon
131 after the first fluorescence signal became detectable (**Figure 2A-C**). Polarization of mCit-GEF14
132 occurred less rapidly but reached a similar degree as mCit-GEF3 at stage +1 (**Figure 2B,D, Figure**
133 **S1),** while mCit-GEF4 and mCit-GEF12, exhibited a lower degree of polarization and association
134 with the plasma membrane (**Figure 2B, E, F, Figure S1**). mCit-GEF3 appeared highly
135 concentrated in a circular polar domain, being barely detectable outside this domain (polarity index
136 at cell "+1": 14.4 ± 2.2) (**Figure 2C, Figure S1**). We tested whether the timing of GEF polarization
137 was dependent on the timing of gene expression and analyzed the polarity indices of mCit-GEF3
138 and mCit-GEF4 under the control of estradiol-inducible promoters. In both cases, the earlier gene
139 expression did not result in an earlier RHID polarization of the protein (**Figure S1**), but rather
140 delayed the time point of significant polarization of mCit-GEF4, likely due to higher cytosolic levels
141 that affected the polarity index calculation. Its independence from gene expression indicates that
142 the timing of polarization is an intrinsic feature that may be controlled by further partners of unknown
143 identity.
144 To determine the functional role of the investigated GEFs we analyzed T-DNA insertion lines for
145 phenotypes in root hair initiation and development. Root hair density was used as a measure for
146 the general ability to develop root hairs, distance of the first bulge from the root tip was used to
147 infer delays in the timing of root hair initiation and root hair length was used as measure for
148 regulation of tip growth. Only in *gef3* mutant alleles, root hair density was reduced and root hair
149 initiation was delayed, (**Figure 2G-I**), while hair length seemed only slightly affected (**Figure S2E**).
150 In *gef3-1*, which lacks almost all full length transcript **(Figure S2C)**, the observed phenotypes could
151 be rescued with a GEF3::mCit-GEF3 construct (**Figure 2H, I**), further verifying that loss of GEF3
152 function causes the phenotypes and confirming the functionality of the fusion construct.
153 Furthermore, other mutant alleles of *gef3* showed a similar delay in root hair initiation (**Figure**
154 **S2B,D**). None of the *gef3* T-DNA insertion lines lacked root hairs entirely, pointing towards
155 functional redundancy among GEFs or compensatory mechanisms. A mutant line carrying both
156 *gef3-1* and *rop2-1* alleles did not exhibit a significant increase in phenotype strength (**Figure 2G-**
157 **I**), which indicates that such compensation involves other ROP-GEF combinations present in
158 trichoblasts. Except for *gef3-1* no other *gef* single mutants, including *gef4-2*, exhibited any
159 significant negative effects on bulge distance or root hair density (**Figure 2G-I**), but *gef4-2* lines did
160 show reduced hair length (**Figure S2E**). A combination of *gef3-1* and *gef4-2* exhibited similar root
161 hair density in *gef3-1*, but showed a small increase in distance of the first bulge from the root tip,
162 i.e. stronger delay in hair initiation (**Figure 2G-I**). This phenotypic analysis suggests different, yet
163 overlapping roles for GEF3 and GEF4, where GEF3 is mainly, but not exclusively, responsible for
164 root hair initiation and bulging, while GEF4 is regulating root hair tip growth.
165
166 **GEF3 is required for efficient root hair emergence and polar recruitment of ROP2**

167 We have shown that GEF3 accumulated very specifically at the RHID, preceded ROP2
168 accumulation, and was required for proper root hair development. Therefore, GEF3 was selected
169 as a promising potential regulator of ROP dependent root hair initiation.
170 To determine the temporal relationship of GEF3 and ROP2 recruitment to the RHID in detail,
171 we observed the localization of both proteins at higher resolution over time. We employed a new
172 microfluidic device, termed RootChip-8S, for long-term imaging of growing *Arabidopsis* roots. The
173 RootChip-8S, is an adapted version of previously published RootChip designs [51-53] and consists
174 of eight separate observation chambers that can be individually perfused to provide stable growth
175 conditions and restrict root movement in Z to prevent focal drift (**Figure S3A, B**). The first detectable
176 signal of GEF3::mCit-GEF3 was observed in the transition zone of the root, shortly after the last
177 cell division (**Figures 2 A and 3 A**). Time-lapse imaging showed early targeting of mCit-GEF3 to
178 the rootward cell pole (**Figure 3 A**). As the protein gradually enriched at the RHID over
179 approximately 30 min (**Figure 3 B**), its localization at the rootward cell pole vanished (**Figure 3 A**).
180 The GEF3 domain eventually stabilized at a consistent diameter of 9.6 µm (± 2.5 µm; *n*=17;
181 FWHM), with its center 9.0 µm (± 2.2 µm) from the rootward cell pole (**Figure 3 B, Figure S3C**).
182 To validate the earlier RHID accumulation of GEF3 compared to ROP2 through simultaneous
183 visualization in the same cells, we imaged their localization in growing roots co-expressing
184 fluorescently labeled versions of both proteins and found that mCit-GEF3 accumulated at the RHID
185 one stage earlier than mTurquoise2-ROP2 (mTq2-ROP2) (**Figure 3 C**).
186 To test if GEF3 directly influences ROP2 recruitment to the RHID, we expressed mCit-ROP2 in
187 the *gef3-1* T-DNA insertion mutant. Strikingly, we did not observe any significant polarization of
188 mCit-ROP2 in the *gef3-1* mutant (**Figure 3 D, E**). Some cells in *gef3-1* were still able to produce
189 bulges, but these bulges lacked polar ROP2 accumulation (**Figure 3 D, E**). Interestingly, the
190 general membrane association of mCit-ROP2 was unaffected, as the localization appeared similar
191 to that in other cell types. This shows that GEF3 function is required for ROP2 recruitment
192 specifically to the RHID. We thus hypothesized that the observed root hair phenotypes in *gef3*
193 mutants could be explained by failed polar recruitment and activation of downstream ROPs.
194 Consequently, ROP loss-of-function mutants would exhibit similar phenotypes as *gef3*. We
195 combined two previously described T-DNA lines for ROP2 and ROP4 [35, 54], and analyzed single
196 and double mutants for phenotypes in root hair initiation. To account for the different genetic
197 backgrounds of both single mutants (*rop2-1*, Col-0; *rop4-1*, WS), we transformed the double mutant
198 *rop2-1/rop4-1* with a ROP2p::mTq2-ROP2 construct, and used the generated line as control for
199 phenotype analysis. For both traits, root hair density and distance of the first bulge to the root tip,
200 the double mutant *rop2-1/rop4-1* showed a phenotype that exceeded the strength of phenotypes
201 in *gef3-1* (**Figure 3 F - H, Figure S2F,G**). The single mutant lines *rop2-1 and rop4-1* showed,
202 however, no significant effects and our ROP2p::mTq2-ROP2 construct was able to fully revert
203 phenotypes in *rop2-1/rop4-1*, demonstrating functional redundancy among both ROPs. In contrast
204 to the loss of ROP2 polarity in *gef3-1* mutants, polar mCit-GEF3 domains were still observed in
205 *rop2-1/rop4-1* mutants (**Figure 3 I, J**). mCit-GEF3 polarity was unaffected in the early elongation

206 zone (**Figure 3 I, J; stage -4**), but was slightly reduced in later stages (**Figure 3 I, J; stages -1,**
207 **+1**) compared to mCit-GEF3 polarity in Col-0 background (**Figure S1**). This indicates that initial
208 GEF3 polarization is largely ROP independent, while ROPs have a positive effect on GEF3 polarity
209 in later stages of root hair development. The question remained how GEF3 fulfills its function as a
210 factor directing polarization of ROP2. Previous studies have demonstrated that GEF-catalyzed
211 nucleotide exchange of ROPs involves the formation of a stable G protein-GEF complex [55-58].
212 To test if GEF3 was capable of recruiting ROP2 through physical interaction, we used a ratiometric
213 bimolecular fluorescence complementation (rBiFC) assay with GEF3 fused to a C-terminal
214 fragment of YFP (cYFP) and either an N-terminal fragment of YFP (nYFP)-carrying ROP2 (wild-
215 type), a constitutively active CA-ROP2 (G14V), a dominant-negative DN-ROP2 (D120A), or a
216 truncated *rop2*ΔN (Δ1-79) that lacks its interaction domain (**Figure S3D**) [5, 59], co-expressed
217 transiently in *Nicotiana benthamiana* leaf epidermis cells [60]. All GEF3-cYFP/nYFP-ROP2
218 combinations, except for *rop2*ΔN, resulted in detectable YFP fluorescence (**Figure 3 K, L, Figure**
219 **S3H-J**). This finding was corroborated by a split-ubiquitin assay in yeast [61], testing the same
220 putative interactor combinations. Except for *rop2*ΔN, all forms of ROP2 yielded yeast growth,
221 indicating physical interaction with GEF3 (**Figure S3E-G**). Consistent with the hypothesis that
222 physical interaction with GEF3 is required for polar recruitment of ROP2 to the RHID, mCit-*rop2*ΔN
223 expressed in *Arabidopsis* trichoblasts did not assume polar localization at the RHID (stage +1,
224 **Figure 3 M, N**). Our interaction assays show further that GEF3 physically interacts with the active
225 as well as the inactive form of ROP2 via its interaction domain. While physical interaction between
226 GEF3 and CA-ROP2 was unexpected at first, specific binding of certain RopGEFs to both, GDP-
227 and GTP-bound ROPs has been demonstrated before [43].
228 Taken together, these results show that GEF3 is necessary for ROP polarization by recruiting
229 ROP2 to the RHID via direct physical interaction. Furthermore, the presence of ROP2 and ROP4
230 is not needed for GEF3 polarization, but enhances GEF3 polarity.
231
232 **GEF3 defines the RHID and guides ROP polarization**
233 To investigate whether GEF3 is not only necessary but also sufficient for ROP2 polarization, we
234 studied transgenic lines, inducibly overexpressing mCit-GEF3 (mCit-GEF3ox) in Col-0 or in
235 ROP2::mTq2-ROP2 background. Upon induction of mCit-GEF3 expression we observed that
236 additional patch-like GEF3 domains formed in trichoblasts and, surprisingly, also in atrichoblasts
237 (**Figure 4 A**). We frequently found mCit-GEF3 accumulation at the shootward sides of cells in the
238 meristem or the early elongation zone (**Figure 4 A**). Importantly, all observed normal and ectopic
239 mCit-GEF3 accumulations resulted in the simultaneous recruitment of mTq2-ROP2 (**Figure 4 A**).
240 We took advantage of the ubiquitous overexpression of mCit-GEF3 and determined its
241 localization in cells outside the root. In epidermal cells of the hypocotyl, we occasionally observed
242 occurrences of ectopic GEF3 accumulation into domains that strikingly resembled those of RHIDs
243 in trichoblasts (**Figure 4 B, Figure S4A**). Consistently, these ectopic mCit-GEF3 domains also lead
244 to recruitment of mTq2-ROP2, which never occurred in hypocotyl cells under control conditions

245 (**Figure 4 B**). Except for trichoblasts, mCit-GEF3ox did not lead to bulge formation in other cells,
246 neither did induced expression of mCit-GEF3ox influence the timing of bulging (**Figure S4B**),
247 indicating that ROP polarization alone was not sufficient to trigger outgrowth and further trichoblast-
248 specific factors are required.

249 Since the analysis of gene expression, protein localization and loss-of-function phenotypes all
250 suggested a differential timing of GEF3 and GEF4 function, we hypothesized that gain-of-function
251 phenotypes should also reflect their specific roles in root hair initiation and growth. We therefore
252 compared the phenotypic effects of mCit-GEF3ox to mCit-GEF4ox, which is known to induce root
253 hair branching in trichoblasts [62]. In mCit-GEF4ox lines, bulges with branched tips, which failed to
254 form long tube-like hairs, occurred in 30.5% of the observed cells (**Figure 4 C, D**). mCit-GEF3ox
255 roots also displayed root hairs with branched tips in 20.6% of all trichoblasts, resembling mCit-
256 GEF4 overexpression (**Figure 4 C, D**). However, mCit-GEF3ox further led to the formation of
257 additional bulges, with 5.5% of trichoblasts showing multiple unbranched bulges and 21.4% of the
258 cells showing multiple branched bulges within one cell (**Figure 4 C, D**). This phenotype bears
259 striking similarities to *scn1* mutants that lack a ROP-inhibiting RhoGDI [11], which further points
260 towards a gain of ROP activity in mCit-GEF3ox roots at an early stage during RHID positioning.
261 We observed mCit-GEF3 accumulations in tips of branched root hairs and mTq2-ROP2 was
262 generally present in the same locations (**Figure 4 E**), thus confirming that mCit-GEF3ox was also
263 responsible for the formation of additional polar domains in branching hairs. These differential
264 effects of GEF3 and GEF4 overexpression resemble the differential timing of their polar localization
265 and further support the hypothesis that both proteins serve specific functions during different
266 phases of root hair development, with GEF3 being decisive for the early formation of the RHID and
267 ROP2 recruitment, and GEF4 being involved in downstream activation of ROP2 to trigger growth.
268

269 **GEFs serve as positional cues during cell polarization**

270 To our knowledge, GEF3 is not only the first RopGEF member reported to temporally precede
271 ROP polarization during tip growth initiation, but it is also the first example for a plant protein that,
272 when overexpressed, is capable of inducing the ectopic formation of polar, ROP-recruiting
273 domains. Our finding, that GEF3 acts upstream of ROP2, challenges the idea of ROP self-
274 organization during the initiation of cell polarization in trichoblasts [63]. A self-organizing reaction-
275 diffusion mechanism, involving the interplay of ROP-activating RopGEFs and ROP-inactivating
276 RopGAPs has been found to underlie the regular cell wall patterning in differentiating metaxylem
277 vessels [64, 65]. In contrast to the multiple, regularly spaced cell wall pits of the metaxylem, the
278 dependable positioning and establishment of a single polar RHID in trichoblast is likely to require
279 a mechanism that eliminates randomness during its formation. Our results suggest that such non-
280 random polarization can be achieved through a GEF3-mediated recruitment and temporally
281 controlled ROP activation by differentially timed GEFs at a predefined location.

282 Evidence for a GTPase-positioning function of GEFs can also be found in other organisms.
283 Recent work shows that during cellularization in Drosophila embryos, the GEF Dizzy and the

heteromeric GEF complex ELMO-Sponge are required for polarization of the GTPase Rap1 [41, 66]. It remains, however, challenging to establish the molecular sequence of GEF and GTPase functions in the context of a developing embryo. In budding yeast, Cdc42 is activated by its GEF Cdc24 during both budding and shmoo formation [67-69]. To initiate budding in yeast, the GEF Bud5 is recruited to the edge of the previous cell-division site by the landmark Axl2 [70]. Stabilized by scaffold proteins, Bud5 and the GEF Cdc24 then locally activate the GTPases Rsr4 and Cdc42 [71-76].

Using a GEF-scaffold complex as landmark for the targeted deployment of the growth machinery may therefore represent a common design principle among eukaryotic cells to prevent spontaneous and random polarization and, instead, drive growth in a directed manner. Yet, the fact that RopGEFs share no conserved features with animal or fungal GEFs [42], indicates that the problem of robust cell morphogenesis has been solved several times during evolution to account for specific differences in cellular growth mechanisms, organ development and lifestyle.

ACKNOWLEDGMENTS

We are grateful to Dominique Bergmann (Stanford) and Sheila McCormick (UC Berkeley) for detailed comments on our manuscript. We thank Karin Schumacher (U. Heidelberg) and Thomas Dresselhaus (U. Regensburg) for helpful advice, all members of the Grossmann lab and our colleagues at COS Heidelberg for inspiring discussions and their active support. We thank Jan Lohmann (Heidelberg), Markus Grebe (Potsdam), Masa Sato (Kyoto), Tijs Ketelaar (Wageningen), Kateřina Schwarzerová (Prague), Yvon Jaillais (Lyon), and Ueli Grossniklaus (Zurich) for sharing materials and Karin Schumacher and Thomas Holstein (both Heidelberg) for access to microscopes. This work was supported by research group funds from the excellence cluster CellNetworks to G.G., grants from the Deutsche Forschungsgemeinschaft (GR 4559/3-1 to G.G. and EV 198/1-1 to J.F.E.), seed funding through the SFB1101, an Emmy Noether fellowship (GR 4251/1-1) to C.G., a PhD-student grant from the Carl-Zeiss-Stiftung to D.G.M., and financial support by ETH Zürich to C.E.S.

AUTHOR CONTRIBUTIONS

The study was conceived by P.D. and G.G.; P.D., A.R., V.A.F.S., D.G.M., L.Y.A., and N.F.K. performed experiments; P.D., A.R., V.A.F.S., D.G.M., L.Y.A., C.G. and G.G. analyzed data. C.E.S. and G.G. designed the microfluidic device. J.F.E. designed the spinning disk microscope and gave advice about the imaging procedure. P.D., A.R. and G.G. prepared figures and wrote the manuscript with input from all coauthors. All authors read and approved the final version of the manuscript.

DECLARATION OF INTERESTS

The authors declare no competing interests.

328 **FIGURES AND FIGURE LEGENDS**

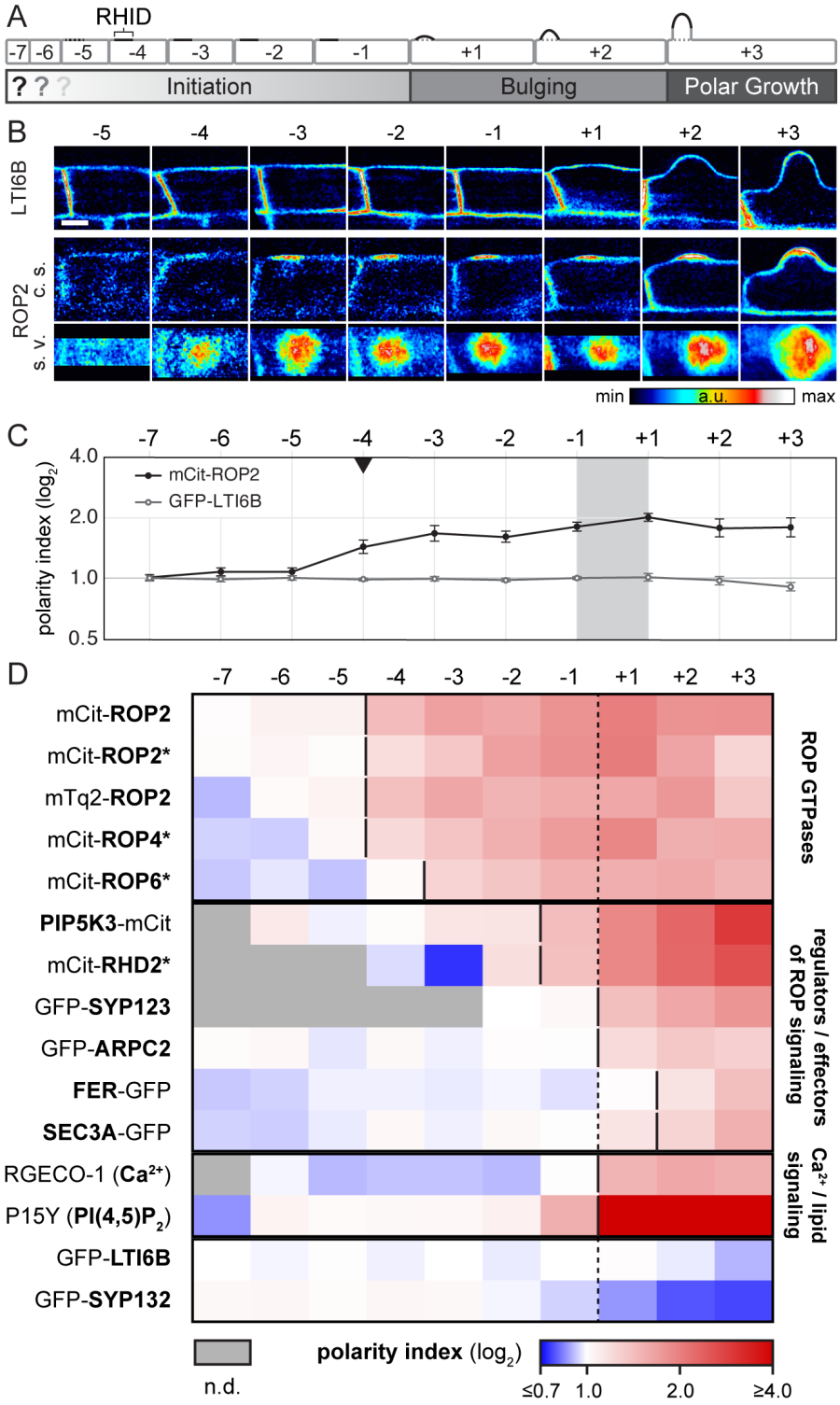

329

330 **Figure 1. Timeline analysis of protein accumulation at the RHID.**

331 (**A**) Model of root hair development in an epidermal cell file. During the initiation phase the root hair
332 initiation domain (RHID) emerges in elongating trichoblasts and the tip growth machinery is
333 assembled using an unknown mechanism. Stages -1/+1 mark the stages before and after the onset
334 of bulging followed by the transition into polar growth. (**B**) Comparison of mCit-ROP2 and GFP-

335 LTI6B protein localization at the RHID in different stages of root hair development. For mCit-ROP2,
336 cross sections (c. s.) and surface views (s. v.) of the same cells are shown. Intensities are
337 represented in false-color, covering the full range of measured values within each data set. Scale
338 bar, 10 µm. (**C**) Polarity index values (signal intensity in/out of RHID; $\log_2$ scale) for mCit-ROP2
339 and GFP-LTI6B along the different root hair stages. Error bars indicate SEM (n(stage -
340 1)=11(ROP2); 14(LTI6B)). The black triangle indicates the first stage with a significant difference
341 between mCit-ROP2 and the evenly distributed GFP-LTI6B ($p < 0.01$). (D) Protein accumulation at
342 the RHID throughout the early development of root hairs in 13 different marker lines. Genes are
343 sorted by the timing of accumulation within their group of protein function. Color coding represents
344 the polarity index for each developmental step. (n.d.: no data). For each stage average polarity
345 index values from multiple cells are shown (see F**igure S1** for details). Stages -7 to -1 represent
346 cells in the initiation phase before bulging, +1 to +3 cells after bulging. Solid vertical lines indicate
347 the first stage with a significant difference between the respective marker and GFP-LTI6B. Listed
348 genes were fused to either eGFP or mCitrine (mCit), under control of their own promoters, except
349 for UBQ10::P15Y (PI(4,5)P_2 reporter), 35S::LTI6B and genes under control of an estradiol inducible
350 promoter (indicated by an asterisk). See also **Figure S1**.

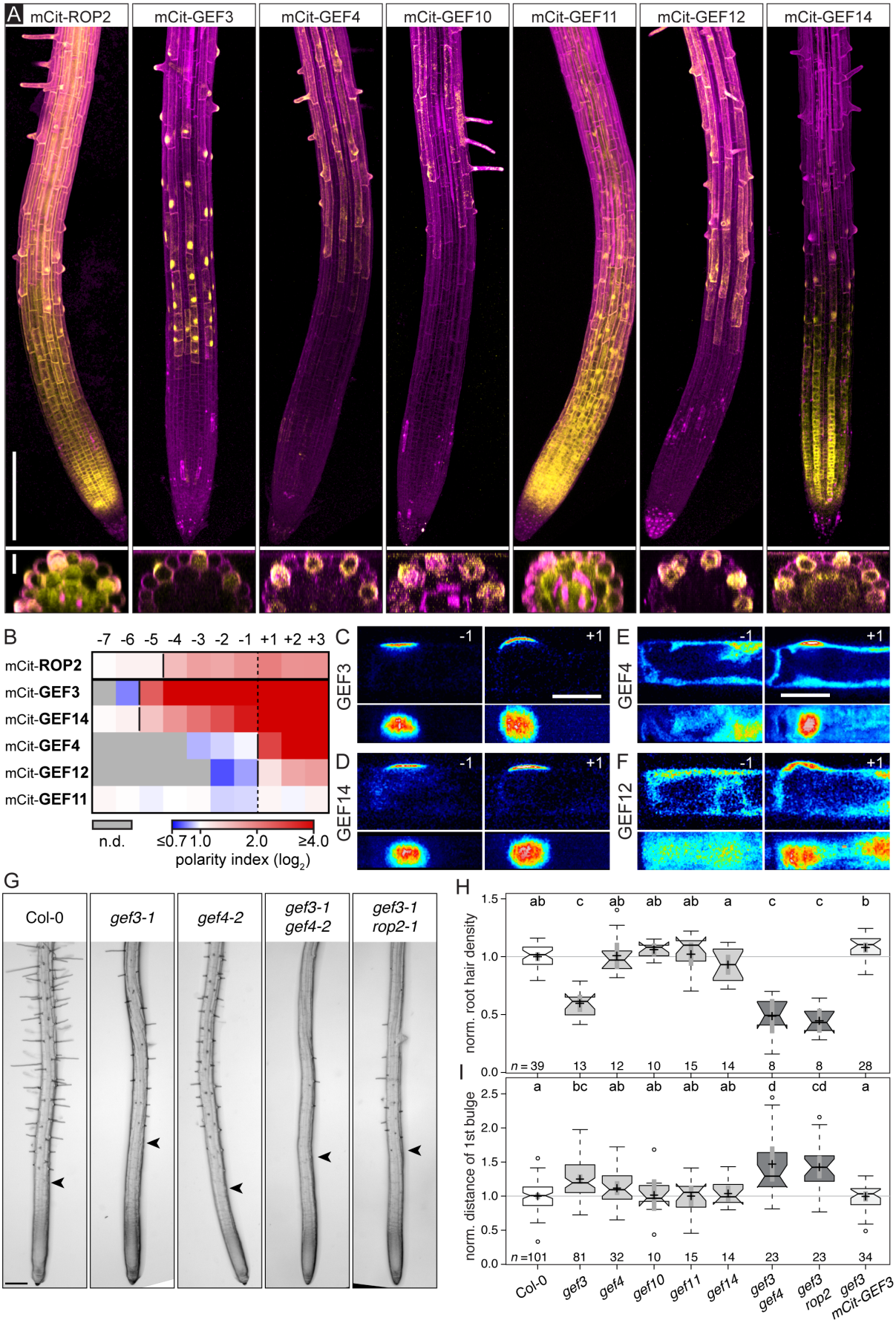
A
mCit-ROP2
mCit-GEF3
mCit-GEF4
mCit-GEF10
mCit-GEF11
mCit-GEF12
mCit-GEF14
B
-7 -6 -5 -4 -3 -2 -1 +1 +2 +3
mCit-ROP2
mCit-GEF3
mCit-GEF14
mCit-GEF4
mCit-GEF12
mCit-GEF11
n.d.
≤0.7 1.0 2.0 ≥4.0
polarity index (log2)
C
GEF3
D
GEF14
E
GEF4
F
GEF12
-1
+1
G
Col-0
gef3-1
gef4-2
gef3-1 gef4-2
gef3-1 rop2-1
H
norm. root hair density
n = 39 13 12 10 15 14 8 8 28
ab c ab ab ab a c c b
I
norm. distance of 1st bulge
n =101 81 32 10 15 14 23 23 34
a bc ab ab ab ab d cd a
Col-0
gef3
gef4
gef10
gef11
gef14
gef3 gef4
gef3 rop2
gef3 mCit-GEF3

351

352 **Figure 2. Functional analysis of RopGEFs in the root epidermis identifies GEF3 to be**
353 **required for efficient root hair emergence.**
354 (**A**) Roots expressing mCit fusion proteins (yellow) under their respective promoters, stained with
355 propidium iodide (magenta) to visualize root and cell outlines. Top panel: Maximum intensity
356 projection of the root tip. Scale bar, 200 µm. lower Panel: Optical cross section through the root in
357 the elongation zone to visualize the tissue-specific expression. Scale bar, 20 µm. (**B**) Timeline
358 analysis of protein accumulation at the RHID for selected GEFs in comparison to ROP2. GEFs are
359 sorted by timing of accumulation at the RHID. Polarity index measurement and calculation as in
360 **Figure 1**. (**C-F**) Subcellular localization (intensity-coded representation) of mCit-GEF3, mCit-
361 GEF4, mCit-GEF14 and mCit-GEF12, in one cell before (-1) and after bulging (+1), respectively.
362 Confocal cross sections (top) and surface views (bottom) of the same cells are shown. Scale bars,
363 20µm. (**G**) Representative root tips of WT (Col-0), and *gef* single and double mutant lines.
364 Arrowheads indicate the first bulge. (**H**, **I**) Quantification of root hair density (**H**) and distance (**I**) of
365 first bulge to the root tip for selected single and double mutants. Values were normalized to
366 corresponding Col-0 values for each independent experiment. Box-plots: number of measurements
367 (n); center lines show medians; notches of boxes represent the 95% confidence interval of the
368 medians; box limits indicate 25th and 75th percentiles as determined by R software; whiskers
369 extend 1.5 times the interquartile range from the 25th and 75th percentiles, dots represent outliers;
370 crosses represent sample means; grey bars indicate 95% confidence intervals of the means.
371 Letters above box-plots show results of an ANOVA-Test (significance value p=0.01), with same
372 letters indicating no significant differences. See also **Figure S2**.
373

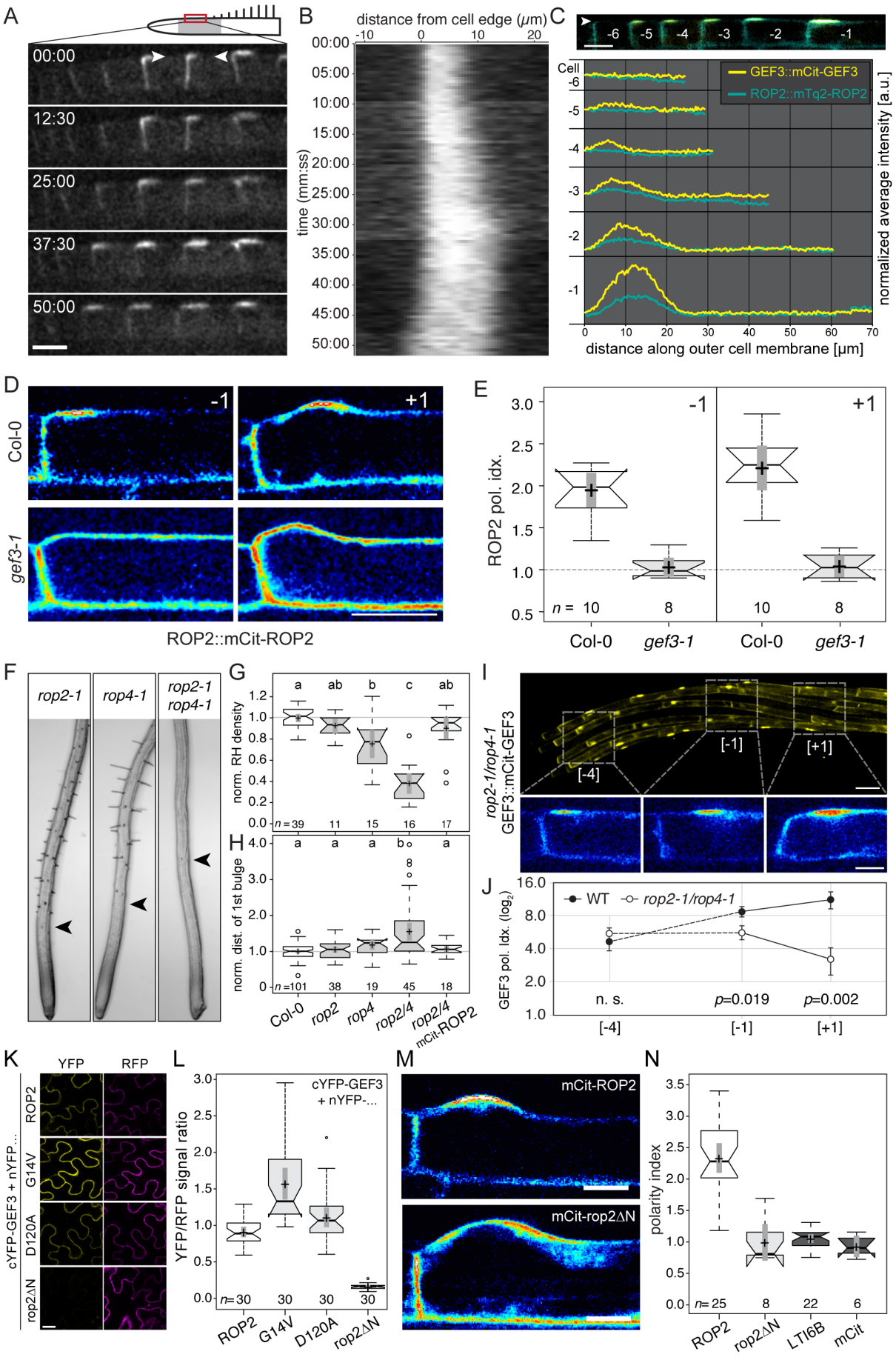
A
00:00
12:30
25:00
37:30
50:00
B
distance from cell edge (μm)
time (mm:ss)
C
Cell
GEF3::mCit-GEF3
ROP2::mTq2-ROP2
normalized average intensity [a.u.]
distance along outer cell membrane [μm]
D
Col-0
gef3-1
ROP2::mCit-ROP2
E
ROP2 pol. idx.
Col-0
gef3-1
F
rop2-1
rop4-1
rop2-1 rop4-1
G
norm. RH density
H
norm. dist. of 1st bulge
Col-0
rop2
rop4
rop2/4
rop2/4 mCit-ROP2
I
rop2-1/rop4-1 GEF3::mCit-GEF3
[-4]
[-1]
[+1]
J
GEF3 pol. Idx. (log2)
WT
rop2-1/rop4-1
n. s.
p=0.019
p=0.002
K
YFP
RFP
cYFP-GEF3 + nYFP...
ROP2
G14V
D120A
rop2ΔN
L
YFP/RFP signal ratio
cYFP-GEF3 + nYFP-...
M
mCit-ROP2
mCit-rop2ΔN
N
polarity index
ROP2
rop2ΔN
LTI6B
mCit

374

375 **Figure 3. GEF3 is necessary for polar ROP2 recruitment during root hair initiation.**
376 (**A**) Time-lapse imaging of GEF3::mCit-GEF3 in the RootChip-8S (see **Figure S2)**. A root hair cell
377 file in the early elongation zone is shown. Multiple stages of protein accumulation can be seen in
378 each still image. The time series was registered to compensate for cell movement due to root
379 growth. Numbers indicate time (mm:ss). Scale bar, 20µm. (**B**) Kymograph of intensity distribution
380 (horizontal axis) along the outer cell flank (left-right orientation) between arrow heads in (**A**) over
381 time (vertical axis). Note the gradual expansion of the emerging mCit-GEF3 domain until
382 approximately 30 min and a stable domain size thereafter. (**C**) Colocalization and intensity profiles
383 of relative signal distribution for mCit-GEF3 and mTq2-ROP2 along root hair cell files. Top: example
384 root hair cell file expressing ROP2::mTq2-ROP2 (cyan) and GEF3::mCit-GEF3 (yellow). Cells are
385 labeled from youngest cells (-6) to oldest cell (-1) before bulging. Bottom: average profiles of
386 relative mTq2-ROP2 (cyan) and mCit-GEF3 (yellow) intensities along the outer cell periphery (line
387 width 3 px) of 6 root hair cell files (arrowhead indicates direction of line measurement). To
388 compensate for intensity differences between measurements, the signal intensities of each
389 construct are normalized to the value at position 0 µm of each cell and afterwards averaged. (**D**)
390 Subcellular localization and (**E**) quantification of mCit-ROP2 polarity at the RHID in Col-0 and the
391 *gef3-1* mutant in root hair cells one cell before (-1) and after bulging (+1). Scale bar, 20µm. (**F**)
392 Representative root tips of *rop2-1*, *rop4-1* and *rop2-1/rop4-1* mutant lines. Arrowheads indicate the
393 first bulge. (**G**, **H**) Quantification of root hair density and distance of first bulge to the root tip in ROP
394 single and double mutants, as well as in *rop2-1/rop4-1* carrying a ROP2::mCit-ROP2 construct.
395 Values are normalized to corresponding Col-0 values for each independent experiment (for
396 comparison, data for Col-0 shown in Figure 2H,I are re-plotted). (**I**) GEF3::mCit-GEF3 expression
397 and localization in *rop2-1/rop4-1* mutant background. Upper panel: overview of the elongation
398 zone. Lower panel: subcellular localization of mCit-GEF3 in cells that correspond to stages -4, -1,
399 and +1. Due to the lack of bulges in this mutant, the reference point used in other lines is missing
400 here and stage designations are therefore estimates. (**J**) Quantification of the polarity index of
401 GEF3::mCit-GEF3 in *rop2-1/rop4-1* mutant background. Stages are chosen as indicated in (**I**). (**K**)
402 Representative images of an rBiFC assay in tobacco epidermal cells for each combination tested.
403 Positive YFP signal indicates protein-protein interaction, RFP signal in the same cells serves as
404 expression control (see Materials and Methods and **Figure S2** for details). All images were
405 recorded using identical conditions and settings, correction for brightness and contrast during
406 image processing was kept equal except for the exemplary YFP image of *rop2*ΔN, which was set
407 brighter to visualize the very low background signal. (**L**) Quantification of ratiometric BiFC
408 experiments. YFP signals were normalized to the corresponding RFP signal to allow comparison
409 of interaction strength. (**M**) Confocal image of root hair cells expressing estradiol inducible mCit-
410 *ROP2* or mCit-*rop2*Δ*N*. Scale bar, 10µm. (**N**) Quantification of polarity index of the constructs
411 shown in (**N**) and compared to the non-polar membrane marker GFP-LTI6B and free mCitrine. For
412 a detailed explanation of all shown box-plots, see the description given in the legend of Figure 2.
413 See also **Figure S3**.

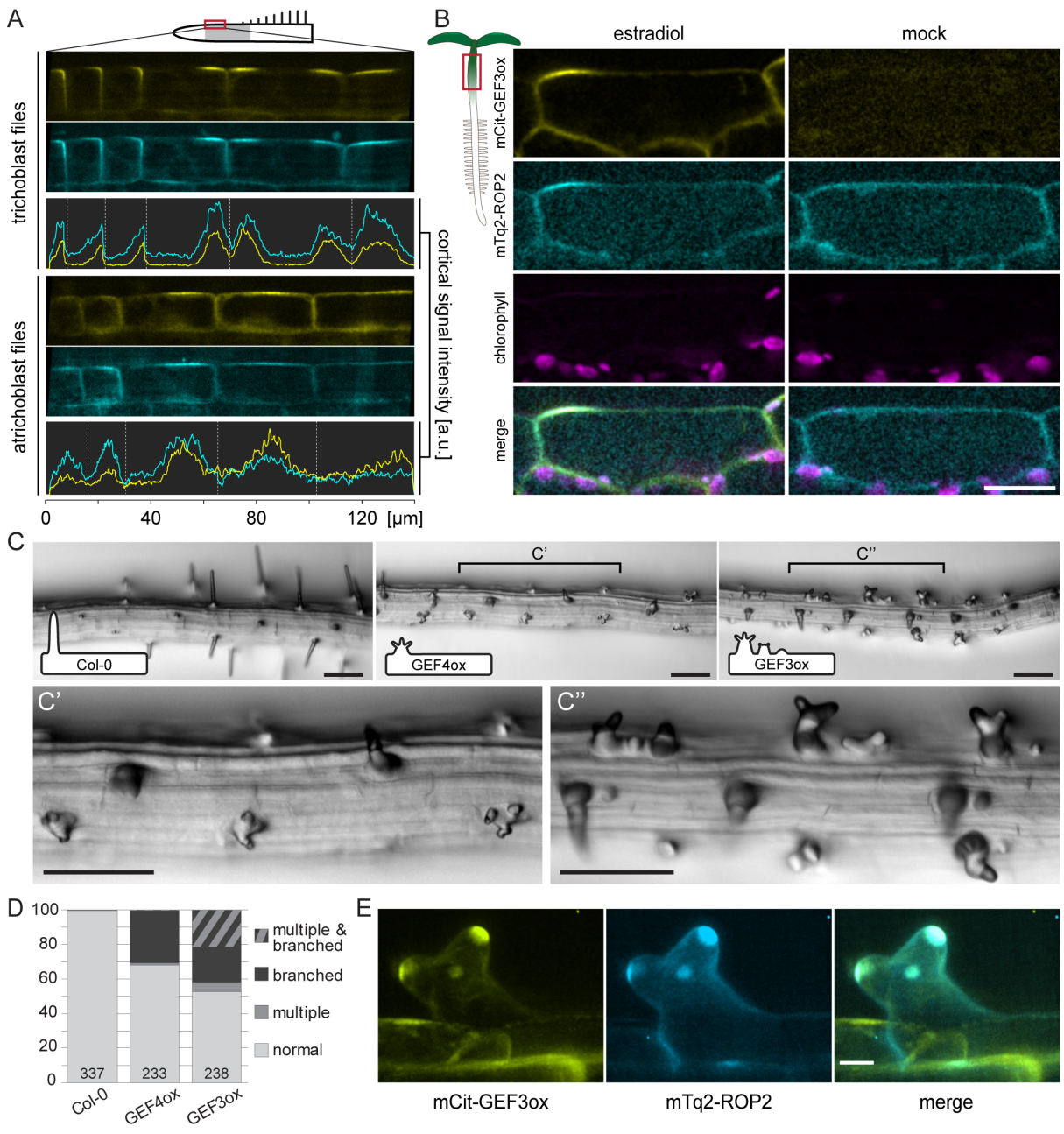

Figure 4. GEF3 initiates the formation of polar growth domains

(**A**) Localization of *ROP2*::mTq2-ROP2 (cyan) in roots overexpressing mCit-GEF3 (yellow). Top: representative cell files of trichoblasts and atrichoblasts, both show ectopic accumulations of both markers. Bottom: intensity profiles along cell periphery of cells shown on the left. Dashed lines indicate cell borders. (**B**) Subcellular localization of *ROP2*::mTq2-ROP2 (cyan) in hypocotyl cells ectopically expressing mCit-GEF3 (yellow). To visualize the background signal in the mCit channel of the mock-treated seedling, intensities were 10-fold enhanced during image processing as compared to the image of estradiol-treated specimen. Other channels are scaled identically. Scale bar, 20 µm. (**C**) Top panels: Representative images of Col-0 (left) and roots overexpressing mCit-*GEF4* (middle) and mCit-*GEF3* (right) (24h after estradiol induction). Inserts show an idealized sketch of the predominant root hair shape. Bottom panels: Higher magnification views of the root

427 zones indicated as C' and C'' in the top panels of GEF4ox and GEF3ox, respectively. Scale bars,
428 100 µm. (**D**) Frequency of phenotypes (induction of multiple hairs, branched bulges, and combined
429 phenotypes) induced by overexpression of lines shown in (**C**) in % of total observed hairs. Bottom
430 numbers indicate *n*. (**E**) Colocalization of mCit-GEF3 (yellow) and ROP2::mTq2-ROP2 (cyan) in
431 branched root hairs, 24 hours after estradiol induction of mCit-GEF3 overexpression. Scale bar,
432 20 µm. See also **Figure S4**.
433

434 **MATERIALS AND METHODS**

435

436 **Plant material**

437 *Arabidopsis thaliana* ecotype Col-0 was used as wildtype in this study. The mutant lines *rop2-1*
438 (SALK_055328C), *gef3-1* (SALK_079879C), *gef3-2* (SALK_079885), *gef3-3* (SAIL_294_A09),
439 *gef3-4* (SALK_021751), *gef3-5* (SALK_046978C), *gef4-2* (SALK_107520) *gef10-1*
440 (SALK_009456), *gef11-1* (SALK_126725C), *gef14-2* (SALK_046067) were obtained from NASC
441 (Nottingham Arabidopsis Stock Centre http://arabidopsis.info/). The *rop4-1* mutant [36] was kindly
442 provided by Markus Grebe (Potsdam). Double mutants were made by crossing and selection for
443 double homozygous plants by PCR (Primers used for genotyping, see Table S3). The GFP-
444 SYP123 and GFP-SYP132 lines [26] were kindly provided by Masa H. Sato (Kyoto), SEC3A-GFP
445 lines [27] were kindly provided by Tijs Ketelaar (Wageningen), the GFP-ARPC2A line [25] was
446 kindly provided by Kateřina Schwarzerová (Prague), and the PI(4,5)P_2-reporter line (P15Y) [31]
447 was kindly provided by Yvon Jaillais (Lyon). To generate transgenic Col-0 lines expressing GFP-
448 tagged FER, Col-0 was transformed with pFER::FER-GFP containing pMDC111 [77], kindly
449 provided by Ueli Grossniklaus (Zurich).
450 Information on all genes referenced in this work, including mutant alleles and sources is provided
451 in **Supplementary Data S1**, **Table S1**.

452

453 **RNA extraction and expression analysis**

454 Seedlings were grown on mesh on a ¼ MS plate. Root tissue was harvested 10 dag, immediately
455 frozen in liquid nitrogen and ground in a tissue lyser (Qiagen) with metal beads. Total RNA was
456 extracted using the RNeasy Plant Mini Kit (Qiagen). After DNAse digest (Thermo Fischer
457 Scientific), 0.5 µg total RNA was used for cDNA synthesis with oligo(dT) primers (RevertAid First
458 Strand cDNA Synthesis Kit, Thermo Fischer Schientific). To test for the presence of Gef3 mRNA,
459 2µl of this cDNA was used for PCR amplification (40 cycles). The primers used for the expression
460 analysis are listed in Supplementary Information, **Table S2**.
461 Data mining of published cell type-specific gene expression was performed using Genevestigator
462 [78].

463

464 **Growth conditions and inducible expression**

465 Plants were grown under long day conditions (16 h light) at 21°C. Seedlings used for experiments
466 were grown for seven days on ¼ MS medium (pH 5.7) without sucrose, supplied with 0.8% plant
467 agar (Duchefa). Transgenic plants transformed with an estradiol inducible construct were induced
468 by covering with cellulose tissues soaked with ¼ MS medium containing 20 µM Estradiol (Stock 20
469 mM in Ethanol) and 0.01% Silwet L77 for 15 minutes. The time after induction differed between the
470 individual expression constructs and ranged from 3 – 12 h to get sufficient signal for imaging. In

471 general, for imaging of protein localization using inducible expression constructs, time after
472 induction was as low as possible to avoid overexpression artefacts.
473

474 **Plant transformation and selection**

475 The agrobacterium strain GV3101::pMP90RK pre-transformed with the helper plasmid pSoup was
476 used for all transformations of *Arabidopsis thaliana*. Plants were transformed using floral dipping
477 and transgenic T1 plants were recovered after the appropriate selection. Selection of constructs
478 containing mTurquoise2 (mTq2) was done on plates containing 50 µg/ml Kanamycin. T1 Selection
479 of constructs containing mCitrine (mCit) was done on soil spraying 3x within 2 weeks (7 – 21 day
480 old seedlings) with Basta®-Solution containing 200 µg/ml Glufosinate-ammonium and 0.05%
481 Tween20. Further generations were selected on plates containing Basta®-Solution to a
482 concentration of 7.5 µg/ml Glufosinate-ammonium. At least 10 independent transgenic lines per
483 expression construct were recovered and checked for fluorescence. Lines that had clear
484 fluorescence and limited phenotypic anomalies were confirmed by PCR and used for further study.
485

486 **Molecular cloning**

487 All cloning for expression vectors used in Arabidopsis was performed using the GreenGate system
488 [79] and base vector pGGZ003 was used for all expression constructs. A List of all expression
489 constructs including module composition and tagging site is provided in Supplementary
490 Information, **Table S3**. Where internal BsaI (Eco31I) sites were present, they were mutated fusing
491 two PCR fragments, with one mutating the internal BsaI site by an altered primer sequence at this
492 site. After cloning the individual modules into the entry vectors, the complete fragment was checked
493 by sequencing. To confirm the correct assembly of modules into pGGZ003, the presence and
494 orientation was checked by sequencing. As fluorophores, mCitrine (mCit) [80] and mTurqoise2
495 (mTq2) [81] were fused to the gene of interest separated by a short GAGAGA-Linker. mCit was
496 cloned from the Ca^{2+} indicator CerTN-L15, containing the common folding mutations V163A and
497 S175G [82], and made monomeric by introducing the A206K mutation. mTq2 was cloned from the
498 Addgene vector pLifeAct-mTurquoise2 (ID #36201). A List of all primers used for molecular cloning
499 is provided in Supplementary Information, **Table S2**.
500 For estradiol inducible expression constructs [83], the XVE gene was fused to the promoter (635
501 bp) and terminator of *UBI10* (AT4G05320). This expression cassette was cloned in reverse
502 orientation into the entry vector pGGA000 together with the oLexA minimal 35S promoter element.
503 Both elements were separated by a 560 bp spacer. This resulted in a single module that could be
504 used as a promoter module for GreenGate cloning.
505 For expression of genes under control of their native promoter, the following sequences upstream
506 of the start codon were cloned into pGGA000: *GEF3* -1743 bp; *GEF4* -1500 bp; *GEF10* -1534 bp;
507 *GEF11* -1458 bp; *GEF12* -701 bp; *ROP2* -1503 bp; *PIP5K3* -1193 bp.

508 For the mbSUS and rBiFC analysis, constructs (listed in Supplementary Information, **Table S3**)
509 were generated using Gateway technology or the 2in1 cloning system (Grefen and Blatt 2012).
510 Coding sequences were PCR-amplified and inserted via 'BP' recombination into either pDONR207,
511 pDONR221-P1P4, or pDONR221-P3P2, respectively, and confirmed by sequencing. Resulting
512 'Entry constructs' were cloned via 'LR' recombination into Destination vectors for either mbSUS or
513 rBiFC [84].
514

515 **Phenotyping of T-DNA insertion lines and inducible overexpression mutant lines**

516 Primary roots (7 dag) were used for all phenotyping experiments. For phenotyping of T-DNA
517 insertion lines the distance of the first bulge to the root tip was defined. The first visible swelling of
518 the cell outline was defined as first bulge, even when this morphological change was very little. The
519 root hair density was analyzed in the next 2 mm. The root hair length was analyzed measuring root
520 hairs growing perpendicular to the root in a region 3-6 mm away from the root tip. For phenotyping
521 the overexpression lines, roots were induced by spraying with medium containing 20 µM Estradiol.
522 The position of the root tip was marked just after induction and normal growing roots were imaged
523 and analyzed 24-26 hours after induction (h. a. i.). A region approximately 2-4 mm from the root tip
524 was used for the analysis of the overexpression phenotype.
525

526 **Propidium iodide (PI) staining**

527 Primary roots (7 dag) were stained for 5 min in 10 µg/ml propidium iodide (PI; diluted in ¼ MS, from
528 1 mg/ml stock), washed in medium and imaged directly. As PI staining varies substantially between
529 different developmental zones of the root, we employed gamma correction (0.75) exclusively in the
530 PI channel of the images to equalize stronger and weaker stained regions in the final figures (see
531 image processing).
532

533 **Ratiometric Bimolecular Fluorescence analyses (rBiFC)**

534 Agrobacterium-mediated transient transformation of 4-6 week old *N. benthamiana* leaves with 2in1
535 rBiFC constructs was performed as described previously [85]. Fluorescence intensities were
536 recorded 36h post infiltration for approximately 30 images per construct as described in [60]. Ratios
537 between complemented YFP fluorescence and RFP were calculated and plotted using BoxplotR.
538 Immunoblotting verified protein expression utilizing anti-MYC conjugated to peroxidase antibodies
539 and anti-HA peroxidase conjugated antibodies, respectively.
540

541 **Mating-based Split Ubiquitin Assay ('Cyto-SUS')**

542 Bait/Cub fusion and preys/Nub fusions were generated by cloning the coding region for *GEF3* and
543 different *ROP2* versions into the Gateway-compatible vectors pMetOYC-Dest and pNX35-Dest,
544 respectively. These were transformed into haploid yeast strains THY.AP4 (Cub fusion) and

545 THY.AP5 (Nub fusions) as described previously [86]. After mating, diploid yeasts were dropped in
546 10 times OD dilutions on vector- (CSM-Leu-, Trp-, Ura) and interaction-selective media (CSM-Leu-
547 , Trp-, Ura-, Ade-, His-) supplemented with 50 or 500 µM methionine. The non-mutated N-terminal
548 ubiquitin moiety (NubI) was used as positive control, and NubI13G (empty vector) as negative
549 control [84]. Protein expression was verified in haploid yeast using antibodies against the VP16
550 domain for the Cub fusion or the HA epitope tag for the Nub fusions.
551

552 **Microfluidic device (RootChip-8S) fabrication and on-chip plant cultivation**

553 Microfluidic device fabrication and on-chip plant cultivation were performed as described in
554 [87, 88]. Briefly, Arabidopsis seedlings were grown in pipette tips filled with solidified medium and
555 interfaced with poly(dimethylsiloxane) (PDMS) RootChip-8S devices 4-5 days after germination
556 under sterile conditions. Media perfusion through the microfluidic channels was controlled using a
557 peristaltic pump (DNE GmbH; volumetric flow rate in each channel, 5 µl/min).
558

559 **Bright-field and fluorescence imaging**

560 Live-cell fluorescence imaging was performed on a custom-built spinning-disk confocal
561 microscope, consisting of a Nikon Ti-E stand, equipped with 20x multi-immersion (N.A. 0.75) and
562 60x water immersion (N.A. 1.2) objectives (Nikon), a motorized stage (Applied Scientific
563 Instrumentation, USA), a spinning disk with customized hole pattern (CREST Optics, Italy), a
564 motorized filter wheel (Cairn Research, UK), a laser launch (Omicron, Germany), and an EMCCD
565 camera (Photometrics, USA). Image acquisition was operated through Nikon NIS Elements
566 software or Micro-Manager [89]. mCitrine-labeled proteins were excited using a laser emitting at
567 the wavelength of 515 nm; mTq2-labeled proteins were excited at 440 nm. Bandpass filter
568 specifications were CWL (central wavelength) = 542 nm, BW (band width) = 20 nm for mCit
569 emission and CWL = 480 nm, BW = 40 for mTq2. Chlorophyll autofluorescence was recorded using
570 561 nm excitation and emission filter specifications of CWL = 630 nm, BW = 92. Root hair
571 phenotyping was performed by transmitted light microscopy on a Nikon SMZ18 stereo microscope,
572 equipped with SHR Plan Apo 0.5x (N.A. 0.075) and 2x (N.A. 0.3) objectives (Nikon) and an Orca
573 Flash 4.0 sCMOS camera (Hamamatsu, Japan). Imaging of the propidium iodide stained root tips
574 expressing different *GEF*::mCit-*GEF* fusions was performed on a Leica SP5 point scanning
575 confocal microscope with a 20x water immersion objective (N.A 0.7), using 1x Zoom, Pinhole 1AU,
576 1024x1024 pixel scanning field, 400 Hz scanning speed, 2x line average as settings. mCit was
577 excited with the 514 nm line of an Argon-Laser and emission light was collected between 520-550
578 nm. Propidium iodide was exited with a 561 nm laser and emission light was collected between
579 570-650 nm. Both channels were imaged in sequential scans to avoid crosstalk using Hybrid-
580 Detectors (Gain 200). Z-Stacks were acquired with 2 µm step size for 20 X objectives and 0.6 µm
581 for 60/63 X objectives. The top-view of the RHID was reconstructed from Z-Stacks using the built-
582 in function of FIJI (3D-Project with interpolation).

583

584 **Image processing, data analysis and software**

585 All image processing, image analysis and measurements was done using FIJI (ImageJ) [90], further
586 data analysis was done in Microsoft Excel, if not mentioned otherwise. A gaussian filter (radius 0.8
587 px) and a rolling ball (radius 100 px) background subtraction was applied to all shown images. The
588 "Royal" lookup table was used for images shown in intensity pseudo color. Kymographs were
589 generated using the multi-kymograph plugin in FIJI. For images of propidium iodide (PI) staining
590 for visualization of the root outlines, the gamma settings were adjusted to 0.75 to reduce the
591 contrast between weakly and strongly stained regions of the root. The adjustment was only done
592 in the PI channel. The signal of the mCitrine-fusions was not altered.
593 To obtain vertical root cross sections, Z-stacks (voxel size: 0.7568x0.7568x2.0142 μm^3) were
594 processed using the Reslice function in FIJI. Maximum intensity projections of approximately 100
595 µm along the root axis, in a distance of approximately 700 to 1000 µm away from the root tip were
596 generated.
597 Polarity indices were analyzed on the original unprocessed images by measuring in 3 by 15 pixel
598 regions at the RHID, outside the RHID and outside the root, as a background value. Before bulge
599 formation a region approximately 10 µm from the rootward cell edge was used as the RHID. The
600 background value was subtracted from both regions and the value outside the RHID was divided
601 by the value inside the RHID [$(Int_{in} - Int_{bkgd}) / Int_{out} - Int_{Bkgd})$]. This polarity index was calculated for
602 each cell within a root hair file, all files were aligned to the first cell with a visible bulge and the
603 average polarity index for each developmental step was calculated. A signal was defined as polar,
604 if its value differed (p-value <0.05, according to two-tailed t-test with unequal variances) to the
605 polarity index of the membrane marker GFP-LTI6B.
606 To measure GEF3 domain size, intensity profiles along the outer plasma membrane were
607 generated from confocal cross sections of trichoblasts. Since gradually decreasing fluorescence
608 signals impede an unambiguous determination of the outer boundary of polar accumulations,
609 domain size was quantified by measuring the full signal width at half-maximal signal intensity
610 (FWHM; **Figure S3**).
611 Box plots were created using BoxPlotR (http://shiny.chemgrid.org/boxplotr/), an R-based web-tool
612 provided by the Tyers (Montreal) and Rappsilber (Edinburgh) labs. For all plots number of
613 measurements (n) is given. Center lines show the medians; notches of boxes represent the 95%
614 confidence interval of the medians; box limits indicate the 25th and 75th percentiles as determined
615 by R software; whiskers extend 1.5 times the interquartile range from the 25th and 75th percentiles,
616 outliers are represented by dots; crosses represent sample means; bars indicate 95% confidence
617 intervals of the means. As statistical test, t-tests (two-tailed, unequal variances) were performed in
618 Microsoft Excel, ANOVA tests were performed in R and the used script is provided in **Data S1**.

619 **SUPPLEMENTAL INFORMATION**

620

621 **Table S1.** List of identifiers for genes and single mutant alleles used in this study.

622

623 **Table S2.** List of PCR primers used for GreenGate and Gateway cloning.

624

625 **Table S3**. List of used expression vectors.

626

627 **Data S1.** R script for ANOVA/Tukey tests performed on mutant phenotype data.

628 **REFERENCES**

629

630 1. Riquelme, M. (2013). Tip growth in filamentous fungi: a road trip to the apex. Annu Rev
631 Microbiol *67*, 587–609.

632 2. Rounds, C. M., and Bezanilla, M. (2013). Growth Mechanisms in Tip-Growing Plant Cells.
633 Annu Rev Plant Biol.

634 3. Russell, S. A., and Bashaw, G. J. (2017). Axon guidance pathways and the control of gene
635 expression.

636 4. Molendijk, A. J., Bischoff, F., Rajendrakumar, C. S., Friml, J., Braun, M., Gilroy, S., and
637 Palme, K. (2001). Arabidopsis thaliana Rop GTPases are localized to tips of root hairs and
638 control polar growth. EMBO J *20*, 2779–2788.

639 5. Jones, M. A., Shen, J.-J., Fu, Y., Li, H., Yang, Z., and Grierson, C. S. (2002). The
640 Arabidopsis Rop2 GTPase is a positive regulator of both root hair initiation and tip growth.
641 Plant Cell *14*, 763–776.

642 6. Bi, E., and Park, H.-O. (2012). Cell polarization and cytokinesis in budding yeast. Genetics
643 *191*, 347–387.

644 7. Ikeda, Y., Men, S., Fischer, U., Stepanova, A. N., Alonso, J. M., Ljung, K., and Grebe, M.
645 (2009). Local auxin biosynthesis modulates gradient-directed planar polarity in
646 Arabidopsis. Nat Cell Biol *11*, 731–738.

647 8. Fischer, U., Ikeda, Y., Ljung, K., Serralbo, O., Singh, M., Heidstra, R., Palme, K., Scheres,
648 B., and Grebe, M. (2006). Vectorial information for Arabidopsis planar polarity is mediated
649 by combined AUX1, EIN2, and GNOM activity. Curr Biol *16*, 2143–2149.

650 9. Kiefer, C. S., Claes, A. R., Nzayisenga, J.-C., Pietra, S., Stanislas, T., Hüser, A., Ikeda, Y.,
651 and Grebe, M. (2015). Arabidopsis AIP1-2 restricted by WER-mediated patterning
652 modulates planar polarity. Development *142*, 151–161.

653 10. Fu, Y., Li, H., and Yang, Z. (2002). The ROP2 GTPase controls the formation of cortical
654 fine F-actin and the early phase of directional cell expansion during Arabidopsis
655 organogenesis. Plant Cell *14*, 777–794.

656 11. Carol, R. J., Takeda, S., Linstead, P., Durrant, M. C., Kakesova, H., Derbyshire, P., Drea,
657 S., Zárský, V., and Dolan, L. (2005). A RhoGDP dissociation inhibitor spatially regulates
658 growth in root hair cells. Nature *438*, 1013–1016.

659 12. Chang, F., Gu, Y., Ma, H., and Yang, Z. (2013). AtPRK2 Promotes ROP1 Activation via
660 RopGEFs in the Control of Polarized Pollen Tube Growth. Mol Plant *6*, 1187–1201.

661 13. Hwang, J.-U., Gu, Y., Lee, Y.-J., and Yang, Z. (2005). Oscillatory ROP GTPase activation
662 leads the oscillatory polarized growth of pollen tubes. Mol Biol Cell *16*, 5385–5399.

663 14. Hwang, J.-U., Vernoud, V., Szumlanski, A., Nielsen, E., and Yang, Z. (2008). A tip-
664 localized RhoGAP controls cell polarity by globally inhibiting Rho GTPase at the cell apex.
665 Curr Biol *18*, 1907–1916.

666 15. Lin, Y., Wang, Y., Zhu, J. K., and Yang, Z. (1996). Localization of a Rho GTPase Implies a
667 Role in Tip Growth and Movement of the Generative Cell in Pollen Tubes. Plant Cell *8*,
668 293–303.

669 16. Yalovsky, S., Bloch, D., Sorek, N., and Kost, B. (2008). Regulation of Membrane

670 Trafficking, Cytoskeleton Dynamics, and Cell Polarity by ROP/RAC GTPases. Plant
671 Physiol *147*, 1527–1543.

672 17. Zhang, Y., and McCormick, S. (2007). A distinct mechanism regulating a pollen-specific
673 guanine nucleotide exchange factor for the small GTPase Rop in Arabidopsis thaliana.
674 Proc Natl Acad Sci USA *104*, 18830–18835.

675 18. Kost, B., Lemichez, E., Spielhofer, P., Hong, Y., Tolias, K., Carpenter, C., and Chua, N. H.
676 (1999). Rac homologues and compartmentalized phosphatidylinositol 4, 5-bisphosphate
677 act in a common pathway to regulate polar pollen tube growth. J Cell Biol *145*, 317–330.

678 19. Cutler, S. R., Ehrhardt, D. W., Griffitts, J. S., and Somerville, C. R. (2000). Random
679 GFP::cDNA fusions enable visualization of subcellular structures in cells of Arabidopsis at
680 a high frequency. Proc Natl Acad Sci USA *97*, 3718–3723.

681 20. Kusano, H., Testerink, C., Vermeer, J. E. M., Tsuge, T., Shimada, H., Oka, A., Munnik, T.,
682 and Aoyama, T. (2008). The Arabidopsis Phosphatidylinositol Phosphate 5-Kinase PIP5K3
683 is a key regulator of root hair tip growth. Plant Cell *20*, 367–380.

684 21. Foreman, J., Demidchik, V., Bothwell, J. H., Mylona, P., Miedema, H., Torres, M. A.,
685 Linstead, P., Costa, S., Brownlee, C., Jones, J. D., et al. (2003). Reactive oxygen species
686 produced by NADPH oxidase regulate plant cell growth. Nature *422*, 442–446.

687 22. Takeda, S., Gapper, C., Kaya, H., Bell, E., Kuchitsu, K., and Dolan, L. (2008). Local
688 positive feedback regulation determines cell shape in root hair cells. Science *319*, 1241–
689 1244.

690 23. Wong, H. L., Pinontoan, R., Hayashi, K., Tabata, R., Yaeno, T., Hasegawa, K., Kojima, C.,
691 Yoshioka, H., Iba, K., Kawasaki, T., et al. (2007). Regulation of Rice NADPH Oxidase by
692 Binding of Rac GTPase to Its N-Terminal Extension. Plant Cell *19*, 4022–4034.

693 24. Mendrinna, A., and Persson, S. (2015). Root hair growth: it's a one way street.
694 F1000Prime Rep *7*, 23.

695 25. Havelková, L., Nanda, G., Martinek, J., Bellinvia, E., Sikorová, L., Šlajcherová, K.,
696 Seifertová, D., Fischer, L., Fišerová, J., Petrásek, J., et al. (2015). Arp2/3 complex subunit
697 ARPC2 binds to microtubules. Plant Science *241*, 96–108.

698 26. Ichikawa, M., Hirano, T., Enami, K., Fuselier, T., Kato, N., Kwon, C., Voigt, B., Schulze-
699 Lefert, P., Baluska, F., and Sato, M. H. (2014). Syntaxin of Plant Proteins SYP123 and
700 SYP132 Mediate Root Hair Tip Growth in Arabidopsis thaliana. Plant Cell Physiol *55*, 790–
701 800.

702 27. Zhang, Y., Immink, R., Liu, C.-M., Emons, A.-M., and Ketelaar, T. (2013). The Arabidopsis
703 exocyst subunit SEC3A is essential for embryo development and accumulates in transient
704 puncta at the plasma membrane. New Phytol *199*, 74–88.

705 28. Xing, S., Mehlhorn, D. G., Wallmeroth, N., Asseck, L. Y., Kar, R., Voss, A., Denninger, P.,
706 Schmidt, V. A. F., Schwarzländer, M., Stierhof, Y.-D., et al. (2017). Loss of GET pathway
707 orthologs in Arabidopsis thaliana causes root hair growth defects and affects SNARE
708 abundance. Proc Natl Acad Sci USA *114*, E1544–E1553.

709 29. Zhao, Y., Araki, S., Wu, J., Teramoto, T., Chang, Y.-F., Nakano, M., Abdelfattah, A. S.,
710 Fujiwara, M., Ishihara, T., Nagai, T., et al. (2011). An expanded palette of genetically
711 encoded Ca^{2+} indicators. Science *333*, 1888–1891.

712 30. Keinath, N. F., Waadt, R., Brugman, R., Schroeder, J. I., Grossmann, G., Schumacher, K.,
713 and Krebs, M. (2015). Live Cell Imaging with R-GECO1 Sheds Light on flg22- and Chitin-
714 Induced Transient $[Ca^{2+}]_{cyt}$ Patterns in Arabidopsis. Mol Plant *8*, 1188–1200.

715 31. Simon, M. L. A., Platre, M. P., Assil, S., van Wijk, R., Chen, W. Y., Chory, J., Dreux, M.,
716 Munnik, T., and Jaillais, Y. (2014). A multi-colour/multi-affinity marker set to visualize
717 phosphoinositide dynamics in Arabidopsis. Plant J *77*, 322–337.

718 32. Duan, Q., Kita, D., Li, C., Cheung, A. Y., and Wu, H.-M. (2010). FERONIA receptor-like
719 kinase regulates RHO GTPase signaling of root hair development. Proc Natl Acad Sci
720 USA *107*, 17821–17826.

721 33. Lin, D., Nagawa, S., Chen, J., Cao, L., Chen, X., Xu, T., Li, H., Dhonukshe, P., Yamamuro,
722 C., Friml, J., et al. (2012). A ROP GTPase-dependent auxin signaling pathway regulates
723 the subcellular distribution of PIN2 in Arabidopsis roots. Curr Biol *22*, 1319–1325.

724 34. Jeon, B. W., Hwang, J. U., Hwang, Y., Song, W. Y., Fu, Y., Gu, Y., Bao, F., Cho, D.,
725 Kwak, J. M., Yang, Z., et al. (2008). The Arabidopsis Small G Protein ROP2 Is Activated
726 by Light in Guard Cells and Inhibits Light-Induced Stomatal Opening. Plant Cell *20*, 75–87.

727 35. Xu, T., Wen, M., Nagawa, S., Fu, Y., Chen, J.-G., Wu, M.-J., Perrot-Rechenmann, C.,
728 Friml, J., Jones, A. M., and Yang, Z. (2010). Cell surface- and rho GTPase-based auxin
729 signaling controls cellular interdigitation in Arabidopsis. Cell *143*, 99–110.

730 36. Fu, Y., Gu, Y., Zheng, Z., Wasteneys, G., and Yang, Z. (2005). Arabidopsis interdigitating
731 cell growth requires two antagonistic pathways with opposing action on cell
732 morphogenesis. Cell *120*, 687–700.

733 37. Li, H., Lin, Y., Heath, R. M., Zhu, M. X., and Yang, Z. (1999). Control of pollen tube tip
734 growth by a Rop GTPase-dependent pathway that leads to tip-localized calcium influx.
735 Plant Cell *11*, 1731–1742.

736 38. Bourne, H. R., Sanders, D. A., and McCormick, F. (1990). The GTPase superfamily: a
737 conserved switch for diverse cell functions. Nature *348*, 125–132.

738 39. Hodge, R. G., and Ridley, A. J. (2016). Regulating Rho GTPases and their regulators. Nat
739 Rev Mol Cell Biol *17*, 496–510.

740 40. Hwang, J.-U., Wu, G., Yan, A., Lee, Y.-J., Grierson, C. S., and Yang, Z. (2010). Pollen-
741 tube tip growth requires a balance of lateral propagation and global inhibition of Rho-family
742 GTPase activity. J Cell Sci *123*, 340–350.

743 41. Schmidt, A., Lv, Z., and Großhans, J. (2018). ELMO and Sponge specify subapical
744 restriction of Canoe and formation of the subapical domain in early Drosophila embryos.
745 Development *145*, dev157909.

746 42. Berken, A., Thomas, C., and Wittinghofer, A. (2005). A new family of RhoGEFs activates
747 the Rop molecular switch in plants. Nature *436*, 1176–1180.

748 43. Gu, Y., Li, S., Lord, E. M., and Yang, Z. (2006). Members of a novel class of Arabidopsis
749 Rho guanine nucleotide exchange factors control Rho GTPase-dependent polar growth.
750 Plant Cell *18*, 366–381.

751 44. Qiu, J.-L., Jilk, R., Marks, M. D., and Szymanski, D. B. (2002). The Arabidopsis SPIKE1
752 Gene Is Required for Normal Cell Shape Control and Tissue Development. Plant Cell *14*,
753 101–118.

754 45. Gu, Y., Li, S., Lord, E. M., and Yang, Z. (2006). Members of a Novel Class of Arabidopsis
755 Rho Guanine Nucleotide Exchange Factors Control Rho GTPase-Dependent Polar
756 Growth. Plant Cell *18*, 366–381.

757 46. Guan, Y., Guo, J., Li, H., and Yang, Z. (2013). Signaling in Pollen Tube Growth: Crosstalk,
758 Feedback, and Missing Links. Mol Plant *6*, 1053–1064.

759 47. Yanagisawa, M., Alonso, J. M., and Szymanski, D. B. (2018). Microtubule-Dependent
760 Confinement of a Cell Signaling and Actin Polymerization Control Module Regulates
761 Polarized Cell Growth. Curr Biol *28*, 2459–2466.e4.

762 48. Birnbaum, K., Shasha, D. E., Wang, J. Y., Jung, J. W., Lambert, G. M., Galbraith, D. W.,
763 and Benfey, P. N. (2003). A gene expression map of the Arabidopsis root. Science *302*,
764 1956–1960.

765 49. Brady, S. M., Orlando, D. A., Lee, J.-Y., Wang, J. Y., Koch, J., Dinneny, J. R., Mace, D.,
766 Ohler, U., and Benfey, P. N. (2007). A high-resolution root spatiotemporal map reveals
767 dominant expression patterns. Science *318*, 801–806.

768 50. Borges, F., Gomes, G., Gardner, R., Moreno, N., McCormick, S., Feijó, J. A., and Becker,
769 J. D. (2008). Comparative Transcriptomics of Arabidopsis Sperm Cells. Plant Physiol *148*,
770 1168–1181.

771 51. Grossmann, G., Guo, W.-J., Ehrhardt, D. W., Frommer, W. B., Sit, R. V., Quake, S. R.,
772 and Meier, M. (2011). The RootChip: an integrated microfluidic chip for plant science.
773 Plant Cell *23*, 4234–4240.

774 52. Jones, A. M., Danielson, J. Å., Manojkumar, S. N., Lanquar, V., Grossmann, G., and
775 Frommer, W. B. (2014). Abscisic acid dynamics in roots detected with genetically encoded
776 FRET sensors. eLife *3*, e01741.

777 53. Stanley, C. E., Shrivastava, J., Brugman, R., Heinzelmann, E., van Swaay, D., and
778 Grossmann, G. (2018). Dual-flow-RootChip reveals local adaptations of roots towards
779 environmental asymmetry at the physiological and genetic levels. New Phytol *217*, 1357–
780 1369.

781 54. Kang, E., Zheng, M., Zhang, Y., Yuan, M., Yalovsky, S., Zhu, L., and Fu, Y. (2017). The
782 Microtubule-Associated Protein MAP18 Affects ROP2 GTPase Activity during Root Hair
783 Growth. Plant Physiol *174*, 202–222.

784 55. Thomas, C., Fricke, I., Weyand, M., and Berken, A. (2009). 3D structure of a binary ROP-
785 PRONE complex: the final intermediate for a complete set of molecular snapshots of the
786 RopGEF reaction. Biol Chem *390*, 427–435.

787 56. Thomas, C., Fricke, I., Scrima, A., Berken, A., and Wittinghofer, A. (2007). Structural
788 evidence for a common intermediate in small G protein-GEF reactions. Mol Cell *25*, 141–
789 149.

790 57. Cherfils, J., and Chardin, P. (1999). GEFs: structural basis for their activation of small
791 GTP-binding proteins. Trends Biochem Sci *24*, 306–311.

792 58. Wittinghofer, F. (1998). Ras signalling - Caught in the act of the switch-on. Nature News
793 *394*, 317–.

794 59. Li, H., Shen, J. J., Zheng, Z. L., Lin, Y., and Yang, Z. (2001). The Rop GTPase switch
795 controls multiple developmental processes in Arabidopsis. Plant Physiol *126*, 670–684.

796 60. Grefen, C., and Blatt, M. (2012). A 2in1 cloning system enables ratiometric bimolecular
797 fluorescence complementation (rBiFC). Biotechniques *53*.

798 61. Grefen, C., Obrdlik, P., and Harter, K. (2008). The Determination of Protein-protein
799 Interactions by the Mating-based Split-ubiquitin system (mbSUS). Methods Mol Biol *479*,
800 1–17.

801 62. Huang, G. Q., Li, E., Ge, F.-R., Li, S., Wang, Q., Zhang, C. Q., and Zhang, Y. (2013).
802 Arabidopsis RopGEF4 and RopGEF10 are important for FERONIA-mediated

803 developmental but not environmental regulation of root hair growth. New Phytol *200*,
804 1089–1101.

805 63. Payne, R. J. H., and Grierson, C. S. (2009). A theoretical model for ROP localisation by
806 auxin in Arabidopsis root hair cells. PLoS ONE *4*, e8337.

807 64. Nagashima, Y., Tsugawa, S., Mochizuki, A., Sasaki, T., Fukuda, H., and Oda, Y. (2018). A
808 Rho-based reaction-diffusion system governs cell wall patterning in metaxylem vessels.
809 Sci. Rep. *8*, 11542.

810 65. Oda, Y., Iida, Y., Kondo, Y., and Fukuda, H. (2010). Wood Cell-Wall Structure Requires
811 Local 2D-Microtubule Disassembly by a Novel Plasma Membrane-Anchored Protein. Curr
812 Opin Plant Biol *20*, 1197–1202.

813 66. Bonello, T. T., Perez-Vale, K. Z., Sumigray, K. D., and Peifer, M. (2018). Rap1 acts via
814 multiple mechanisms to position Canoe and adherens junctions and mediate apical-basal
815 polarity establishment. Development *145*, dev157941.

816 67. Peterson, J., Zheng, Y., Bender, L., Myers, A., Cerione, R., and Bender, A. (1994).
817 Interactions between the bud emergence proteins Bem1p and Bem2p and Rho-type
818 GTPases in yeast. J Cell Biol *127*, 1395–1406.

819 68. Nern, A., and Arkowitz, R. A. (1998). A GTP-exchange factor required for cell orientation.
820 Nature *391*, 195–198.

821 69. Zheng, Y., Bender, A., and Cerione, R. A. (1995). Interactions among proteins involved in
822 bud-site selection and bud-site assembly in Saccharomyces cerevisiae. J Biol Chem *270*,
823 626–630.

824 70. Roemer, T., Madden, K., Chang, J., and Snyder, M. (1996). Selection of axial growth sites
825 in yeast requires Axl2p, a novel plasma membrane glycoprotein. Genes & Development
826 *10*, 777–793.

827 71. Chant, J., Corrado, K., Pringle, J. R., and Herskowitz, I. (1991). Yeast BUD5, encoding a
828 putative GDP-GTP exchange factor, is necessary for bud site selection and interacts with
829 bud formation gene BEM1. Cell *65*, 1213–1224.

830 72. Bender, A., and Pringle, J. R. (1989). Multicopy suppression of the cdc24 budding defect
831 in yeast by CDC42 and three newly identified genes including the ras-related gene RSR1.
832 Proc Natl Acad Sci USA *86*, 9976–9980.

833 73. Chiou, J.-G., Balasubramanian, M. K., and Lew, D. J. (2017). Cell Polarity in Yeast. Annu
834 Rev Cell Dev Biol *33*, annurev–cellbio–100616–060856.

835 74. Wedlich-Soldner, R., Wai, S. C., Schmidt, T., and Li, R. (2004). Robust cell polarity is a
836 dynamic state established by coupling transport and GTPase signaling. J Cell Biol *166*,
837 889–900.

838 75. Yamaguchi, Y., Ota, K., and Ito, T. (2007). A Novel Cdc42-interacting Domain of the Yeast
839 Polarity Establishment Protein Bem1 IMPLICATIONS FOR MODULATION OF MATING
840 PHEROMONE SIGNALING. J Biol Chem *282*, 29–38.

841 76. Butty, A. C., Pryciak, P. M., Huang, L. S., Herskowitz, I., and Peter, M. (1998). The role of
842 Far1p in linking the heterotrimeric G protein to polarity establishment proteins during yeast
843 mating. Science *282*, 1511–1516.

844 77. Escobar-Restrepo, J.-M., Huck, N., Kessler, S., Gagliardini, V., Gheyselinck, J., Yang, W.-
845 C., and Grossniklaus, U. (2007). The FERONIA receptor-like kinase mediates male-female
846 interactions during pollen tube reception. Science *317*, 656–660.

847 78. Hruz, T., Laule, O., Szabó, G., Wessendorp, F., Bleuler, S., Oertle, L., Widmayer, P.,
848 Gruissem, W., and Zimmermann, P. (2008). Genevestigator v3: a reference expression
849 database for the meta-analysis of transcriptomes. Adv Bioinformatics *2008*, 420747.

850 79. Lampropoulos, A., Sutikovic, Z., Wenzl, C., Maegele, I., Lohmann, J. U., and Forner, J.
851 (2013). GreenGate---a novel, versatile, and efficient cloning system for plant transgenesis.
852 PLoS ONE *8*, e83043.

853 80. Griesbeck, O., Griesbeck, O., Baird, G. S., Baird, G. S., Campbell, R. E., Campbell, R. E.,
854 Zacharias, D. A., Zacharias, D. A., Tsien, R. Y., and Tsien, R. Y. (2001). Reducing the
855 Environmental Sensitivity of Yellow Fluorescent Protein. J Biol Chem *276*, 29188–29194.

856 81. Goedhart, J., Stetten, von, D., Noirclerc-Savoye, M., Lelimousin, M., Joosen, L., Hink, M.
857 A., van Weeren, L., Gadella, T. W. J., and Royant, A. (2012). Structure-guided evolution of
858 cyan fluorescent proteins towards a quantum yield of 93%. Nat Commun *3*, 509.

859 82. Heim, N., Garaschuk, O., Friedrich, M. W., Mank, M., Milos, R. I., Kovalchuk, Y., Konnerth,
860 A., and Griesbeck, O. (2007). Improved calcium imaging in transgenic mice expressing a
861 troponin C–based biosensor. Nat Meth *4*, 127–129.

862 83. Zuo, J., Niu, Q.-W., and Chua, N.-H. (2000). An estrogen receptor-based transactivator
863 XVE mediates highly inducible gene expression in transgenic plants. Plant J *24*, 265–273.

864 84. Xing, S., Wallmeroth, N., Berendzen, K. W., and Grefen, C. (2016). Techniques for the
865 Analysis of Protein-Protein Interactions in Vivo. Plant Physiol *171*, 727–758.

866 85. Mehlhorn, D. G., Wallmeroth, N., Berendzen, K. W., and Grefen, C. (2018). 2in1 Vectors
867 Improve In Planta BiFC and FRET Analyses. In The Plant Endoplasmic Reticulum
868 Methods in Molecular Biology. (New York, NY: Humana Press, New York, NY), pp. 139–
869 158.

870 86. Asseck, L. Y., Wallmeroth, N., and Grefen, C. (2018). ER Membrane Protein Interactions
871 Using the Split-Ubiquitin System (SUS). In The Plant Endoplasmic Reticulum Methods in
872 Molecular Biology. (New York, NY: Humana Press, New York, NY), pp. 191–203.

873 87. Grossmann, G., Meier, M., Cartwright, H. N., Sosso, D., Quake, S. R., Ehrhardt, D. W.,
874 and Frommer, W. B. (2012). Time-lapse fluorescence imaging of Arabidopsis root growth
875 with rapid manipulation of the root environment using the RootChip. J Vis Exp *65*, e4290.

876 88. Stanley, C. E., Shrivastava, J., Brugman, R., Heinzelmann, E., Frajs, V., Bühler, A., van
877 Swaay, D., and Grossmann, G. (2018). Fabrication and Use of the Dual-Flow-RootChip for
878 the Imaging of Arabidopsis Roots in Asymmetric Microenvironments. Bio-protocol *8*, 1–19.

879 89. Edelstein, A., Amodaj, N., Hoover, K., Vale, R., and Stuurman, N. (2010). Computer
880 control of microscopes using µManager. Curr Protoc Mol Biol *Chapter 14*, Unit14.20.

881 90. Schindelin, J., Arganda-Carreras, I., Frise, E., Kaynig, V., Longair, M., Pietzsch, T.,
882 Preibisch, S., Rueden, C., Saalfeld, S., Schmid, B., et al. (2012). Fiji: an open-source
883 platform for biological-image analysis. Nat Meth *9*, 676–682.